Korean J. Chem. Eng., 37(7), 1258-1265 (2020)
DOI: 10.1007/s11814-020-0537-y

pISSN: 0256-1115
eISSN: 1975-7220

Solid-state conversion of metal oleate precursors for the preparation of $LiNi_{1/3}Co_{1/3}Mn_{1/3}O_2$ as cathode material for lithium-ion batteries

Dongyub Kwak*,‡, Won-Gwang Lim,‡, Kyuchul Shin*, In Woo Cheong*,†, Jinwoo Lee**,†, and Jin Joo*,†**

*Department of Applied Chemistry, Kyungpook National University, Daegu 41566, Korea
**Department of Chemical and Biomolecular Engineering, Korea Advanced Institute of Science and Technology (KAIST), Daejeon 34141, Korea

(*Received 19 January 2020 • Revised 5 March 2020 • Accepted 8 March 2020*)

Abstract−A solid-state conversion process for the preparation of $LiNi_{1/3}Co_{1/3}Mn_{1/3}O_2$ (NCM333) using metal oleate precursors was studied. The low melting points of metal oleate complexes result in a highly homogeneous mixture of Li-, Ni-, Co-, and Mn-oleates before calcination at a high temperature in a solid-state conversion process. The discharge capacity and capacity retention were assessed using a control sample prepared with metal acetate precursors. Cyclic voltammetry and electrochemical impedance spectroscopy showed larger cathodic and anodic peak currents and a lower charge transfer resistance for the coin cell with the cathode prepared from metal oleates than for the cell with the cathode prepared from metal acetates. The superior electrochemical properties of the NCM333 cathode prepared by the solid-state conversion process suggested in this study are attributed to the formation of a perfect $R\bar{3}m$ layered structure with a low degree of cation mixing.

Keywords: Solid-state Conversion, Lithium Ion Battery, Cathode, Cation Mixing, Layered Structure

INTRODUTION

Advancements in Li-ion battery (LIB) technology have led to a recent rapid expansion of the global market for portable electronic devices and electric vehicles [1,2]. Despite such improvements in the electrochemical performance of LIBs, batteries with a higher reversible capacity, greater rate capability, and longer cycle life are still strongly demanded for various applications [3-5]. Among the components of LIBs, the cathode material is a critical part that limits their capacity and cycle life [6,7]. Following the commercialization of layer-structured $LiCoO_2$ as a cathode material, $LiNi_xCo_yMn_zO_2$ ($x+y+z=1$, hereafter denoted as NCM*xyz*) has found great success in industry [8]. NCM exhibits relatively high stability with a larger capacity than other cathode materials such as $LiFePO_4$ and $LiMn_2O_4$ [9-14]. Ni contributes to the capacity of the cathode, Co favors the formation of a layered crystal structure, and Mn enhances the stability of the layered structure during charge and discharge of an LIB. In an industrial process for mass production of NCMs, a continuously stirred-tank reactor (CSTR) is widely used to achieve a homogeneous distribution of these three transition metals within NCM particles via coprecipitation of transition-metal hydroxides [15-21], where transition metal solutions are fed into the CSTR with vigorous mixing of the reaction solution as the pH is maintained at 11-12 [17-21]. However, careful control of the pH level, process time, temperature, and concentration of the transition metals and ammonia under an inert gas is required to produce high-quality NCM materials; a large amount of waste is also produced, increasing production costs. For this reason, various synthesis routes have been explored, including solid-state conversion [22,23], a molten salt method [24,25], sol-gel synthesis [26-28], hydrothermal synthesis [29-31], a polymer template method [32-34], an electrospinning method [35], and a micro-emulsion method [36]. Among them, the direct conversion of reactants in the solid state for the synthesis of NCM has been intensively explored for producing high-quality NCM in a cost-effective manner. The solid-state conversion process is carried out by grinding and mixing transition-metal precursors via ball-milling, followed by calcination at a high temperature; however, ball-milling for an extended period compromises productivity. Moreover, achieving a homogeneous distribution of Li and transition metals within the crystal structure of NCM particles is difficult because of the low diffusion coefficient of metal ions in the solid state. Even though the diffusion of atoms in the solid state can be enhanced by ball-milling, which reduces the precursor particle size and increases the contact area between particles, inhomogeneous mixing of Li and transition metals necessarily leads to poor electrochemical performance of the resulting NCM cathode materials [22,23,37,38]. For example, solid-state conversion of an inhomogeneous mixture often causes the undesirable formation of separate crystal phases with a targeted layered structure of NCM. The disordered phase formation of transition-metal cations (often called cation mixing) is another drawback observed in solid-state conversion, where Ni occupies Li sites in the layered crystal structure (space group $R\bar{3}m$) of NCM [39,40].

In the present work, to address the aforementioned issues, we used metal oleate ($M(OA)_2$, M=Ni, Co, Mn) precursors in the direct conversion of solid-state precursors for NCM materials. The $M(OA)_2$ precursors are complexes of transition metals and oleic acid; they

†To whom correspondence should be addressed.
E-mail: inwoo@knu.ac.kr, jwlee1@kaist.ac.kr, joojin@knu.ac.kr
‡These authors contributed equally to this work.

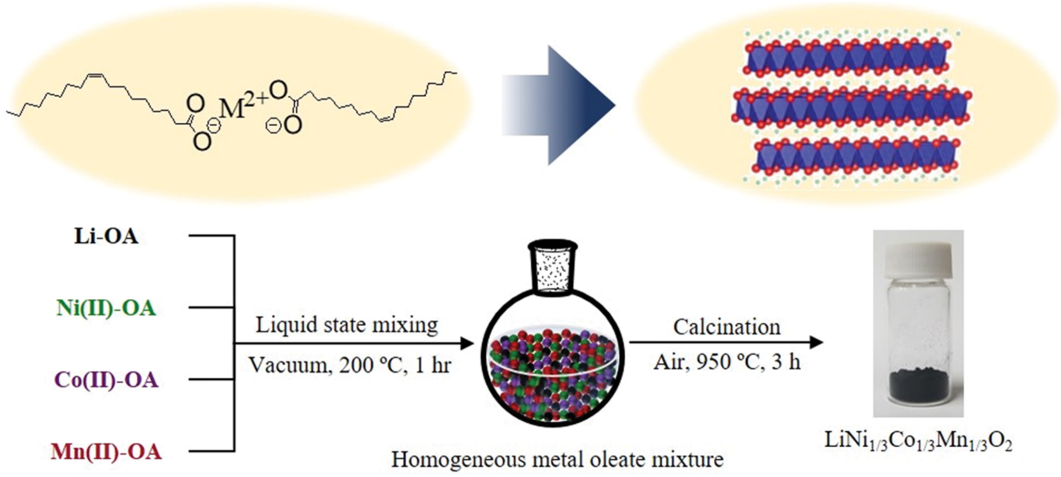

Fig. 1. The illustration showing the synthesis procedure for $LiNi_{1/3}Co_{1/3}Mn_{1/3}O_2$ cathode material using metal oleate precursors.

exhibit melting points as low as ~100-150 °C because of the cis conformation of the double bond in the middle of the OA carbon chain. When a mixture of different $M(OA)_2$ is heated, a highly homogeneous liquid-like mixture is obtained. Calcination of this homogeneous mixture at an elevated temperature gives high-quality NMC with a uniform composition at the atomic level throughout the particles as shown in Fig. 1. To demonstrate this simple and effective procedure for the synthesis of NCM, we studied the solid-state conversion of an $M(OA)_2$ mixture into $LiNi_{1/3}Co_{1/3}Mn_{1/3}O_2$ (NCM333). NCM333 has been widely investigated because it has a moderate charge/discharge capacity and a relatively long cycle life; thus, it is an ideal model for evaluating the efficacy of our synthesis scheme [41-45].

EXPERIMENTAL

1. Synthesis of NCM333 as a Cathode Material

OA (90%, Sigma-Aldrich), $NiCl_2{\cdot}6H_2O$ (98%, Junsei), $CoCl_2{\cdot}6H_2O$ (95%, Junsei), $MnCl_2{\cdot}4H_2O$ (99%, Sigma-Aldrich), and LiOH (98%, Sigma-Aldrich) were used as received without further purification. First, an alkali metal oleate such as sodium oleate (NaOA) or lithium oleate (LiOA) was synthesized by reacting NaOH or LiOH, respectively, and OA. In a typical experiment, 0.5 mol (20 g) of NaOH and 0.6 mmol (169 g) of OA were dissolved in 300 mL of ethanol at room temperature. The solution was heated and the reaction was conducted under reflux for 12 h. After the reaction mixture cooled, the solution was added to an excess of acetone to precipitate the NaOA product. The white precipitate was filtered, rinsed with acetone several times and dried in a vacuum oven. LiOA was synthesized using the same procedure by reacting LiOH and OA. $Ni(OA)_2$ was synthesized by reacting metal chlorides of $NiCl_2$ with NaOA. Forty millimoles of $NiCl_2{\cdot}6H_2O$ and 80 mmol of NaOA were dissolved in a mixture solvent composed of 80 mL ethanol, 60 mL distilled water, and 140 mL hexane. The resulting solution was heated to 70 °C and refluxed for 12 h. After the reaction mixture cooled to room temperature, the upper organic layer containing the $Ni(OA)_2$ complex was washed several times with distilled water in a separatory funnel. The hexane was then evaporated off, yielding a $Ni(OA)_2$ complex in a waxy solid form. $Co(OA)_2$ and $Mn(OA)_2$ were synthesized using the same procedure but with the corresponding metal chlorides and NaOA [46].

For the synthesis of NCM333 with metal oleate precursors via solid-state reaction, a mixture containing LiOA, $Ni(OA)_2$, $Co(OA)_2$, and $Mn(OA)_2$ (Li : Ni : Co : Mn=3.3 : 1 : 1 : 1 molar ratio) was prepared at 200 °C under vacuum for 1 h. Li was used in 10% excess because of the evaporation of Li at high calcination temperatures. The resulting homogeneous mixture was calcined in a muffle furnace at various temperatures to produce the optimum sample (hereafter denoted as NCM-OA). To compare the electrochemical performance of NCM-OA as a cathode material, a control sample were synthesized using metal acetate ($M(Ac)_2$) precursors. The precursors of LiAc, $Ni(Ac)_2$, $Co(Ac)_2$, and $Mn(Ac)_2$ were thoroughly mixed and ground with a mortar for 2 h. The precursor mixture was calcined at 950 °C for 3 h in a muffle furnace, producing NCM333 (hereafter denoted as NCM-Ac).

2. Characterization

Thermogravimetric analysis and differential scanning calorimetric analysis (TGA-DSC) were performed with a TA Instruments Q600 thermal analysis system. The samples were heated from room temperature to 1,000 °C at a heating rate of 10 °C/min in dry air. The phase purity and crystal structure of the calcined samples were investigated using X-ray diffraction (XRD, Rigaku D/Max-2500). The XRD data were collected by step scanning over the 2θ range from 10° to 70° with Cu-Kα radiation generated at 40 kV and 200 mA. Rietveld refinement analysis of the XRD data was conducted with the FullProf Suite software [47,48]. The morphology and microscopic features of NCM-OA and NCM-Ac samples were characterized by field-emission scanning electron microscopy (FE-SEM, Hitachi SU8230). Inductively coupled plasma atomic emission spectroscopy (ICP-AES, PerkinElmer Optima 8300) and energy-dispersive X-ray spectroscopy (EDS) were used to investigate the chemical composition of the NCM-OA and NCM-Ac samples.

3. Electrochemical Measurements

The electrochemical performance of the as-prepared NCM333 samples was evaluated using coin-type half-cells (CR2032). To prepare cathode electrodes, 80 wt% NCM-OA or NCM-Ac (active

material), 10 wt% Super-P carbon black (conductor), and 10 wt% polyvinylidene fluoride (binder, Alfa Aesar) were dispersed in *N*-methyl-2-pyrrolidone (anhydrous, 99.5%, Sigma-Aldrich) to form a homogeneous slurry. The slurry was subsequently coated onto aluminum foil (current collector) using a doctor-blade method and dried in a vacuum oven at 70 °C for at least 12 h to remove remaining solvent and moisture. The dried cathode electrode was then rolled to the appropriate thickness and punched into 12 mm-diameter discs. The coin cells were assembled by sandwiching a 14 mm-diameter polypropylene film (separator, Celgard 2400) between the cathode electrode and a lithium metal anode electrode in an argon-filled glovebox. The organic electrolyte was 1.0 M lithium hexafluorophosphate salt dissolved in a mixed solvent of ethylene carbonate (EC) and dimethyl carbonate (DMC) (1 : 1, v/v) (PANAX ETEC). The galvanostatic charge-discharge performance of the cells was characterized on a battery cycler system (WonATech WBCS3000) in the voltage window from 3.0 to 4.3 V (vs. Li/Li^+) at a C-rate of 0.5C (100 mA h g^{-1}). The rate capability of different cells was measured at various rates of 0.5C, 1C, and 2C. Cyclic voltammetry (CV) and electrochemical impedance spectroscopy (EIS) analyses were conducted using a potentiostat (Reference 600, Gamry Instruments, USA). For the measurements, a two electrode system was prepared by coin cell consisting of NCM333 as working electrode and Li foil as counter/reference electrode. Especially, CV was conducted at a scan rate of 0.1 mV s^{-1} from 3.0 to 4.3 V (vs Li/Li^+) and EIS was conducted at room temperature in the frequency range from 10^5 to 0.01 Hz by applying an AC signal of 10 mV magnitude.

RESULTS AND DISCUSSION

1. Synthesis of NCM333 (NCM-OA)

Fig. 2 shows the XRD patterns of the products of the mixtures of LiOA and $M(OA)_2$ precursors calcined at various temperatures from 450 to 950 °C. The layered $R\bar{3}m$ structure of NCM-OA began to form at temperatures as low as 450 °C, as indicated by the emergence of the (003) reflection peak in Fig. 2. Among the possible calcination products of LiOA, $Ni(OA)_2$, $Co(OA)_2$, and $Mn(OA)_2$ in the reaction mixture, the spinel Co_3O_4 phase has a peak at the same diffraction angle of 18.81° (due to diffraction of its (111) planes) as the (003) peak in the pattern of the layered structure. However, the peak at 18.81° is reasonably attributed to the layered $R\bar{3}m$ phase because the most intense peak from the (311) plane of Co_3O_4, which should appear at 36.93°, is not observed.

Fig. 3 represents the TGA-DSC curves for each metal oleate precursor. LiOA, $Co(OA)_2$, and $Mn(OA)_2$ used in the synthesis of NCM-OA exhibit steep weight losses with intense endothermic peaks at ~500 °C when they are calcined under air, which results from the combustion of the organic oleate ligands in the metal complexes. In the case of $Ni(OA)_2$, thermal decomposition to Ni metal occurs at 200-250 °C. Below the combustion temperature of oleate, the metal oleates show similar melting and thermal decomposition behavior. At temperatures ranging from 150 to 200 °C, the metal oleate precursors become a viscous liquid phase, followed by thermal decomposition, resulting in Li_2CO_3, Ni metal and NiO, CoO and Co_3O_4, and MnO and Mn_3O_4 as the temperature was

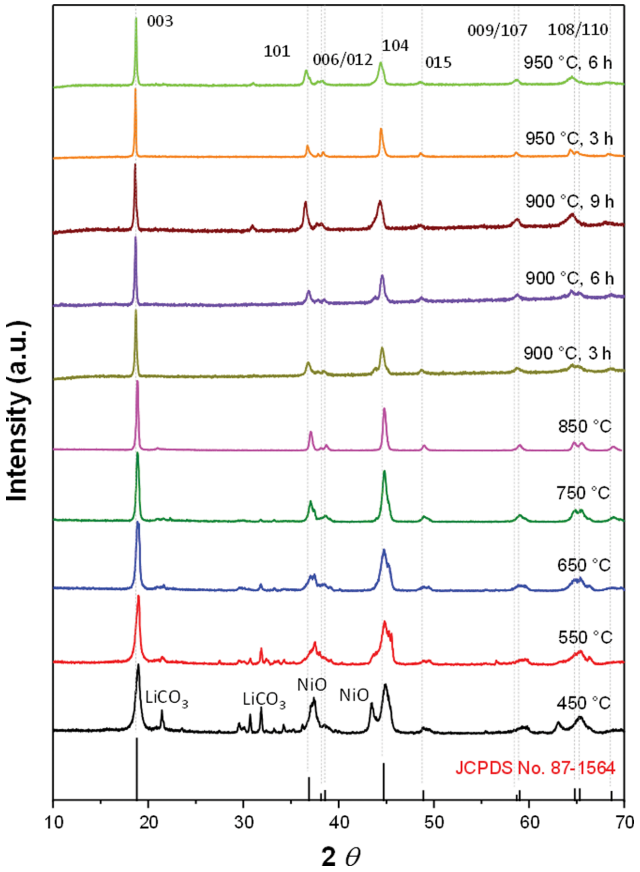

Fig. 2. XRD patterns of NCM-OA prepared by calcination of a mixture composed of LiOA and $M(OA)_2$ precursors at different temperatures.

increased to the oleate decomposition temperature of 500 °C (Fig. S1). The low melting points of the metal oleate precursors are beneficial for achieving a homogeneous mixture at the molecular level without any solvent before they decompose to form oxides, thereby yielding a homogeneous population of Ni, Co, and Mn cations within a particle in the final NCM333 product. Notably, the CSTR process has been widely used to achieve a homogeneous distribution of metal cations within a layered $R\bar{3}m$ structure; however, very careful control over the operating conditions (e.g., pH, feed rate of the precursor solutions, process time, and temperature) is required. The conventional solid-state conversion method requires tedious grinding before calcination to produce a homogeneous mixture; however, a highly homogeneous distribution of metal cations in the layered structure is hardly obtained by using conventional solid state conversion process. In our simple solid-state conversion process using metal oleate precursors, because of their fluidic property at relatively low temperatures, all of the metal ions are well mixed at the molecular level in a short time before they are converted into a layered structure. Also, our newly-proposed process produces very little waste compared to the CSTR process. This method would enable the industrial mass-production of $LiNi_{1/3}Co_{1/3}Mn_{1/3}O_2$.

Another issue to be addressed in the preparation of layered $R\bar{3}m$-structured cathode materials is the replacement of Li^+ with Ni in the Li^+ sites (3b sites), often called cation mixing. Such cat-

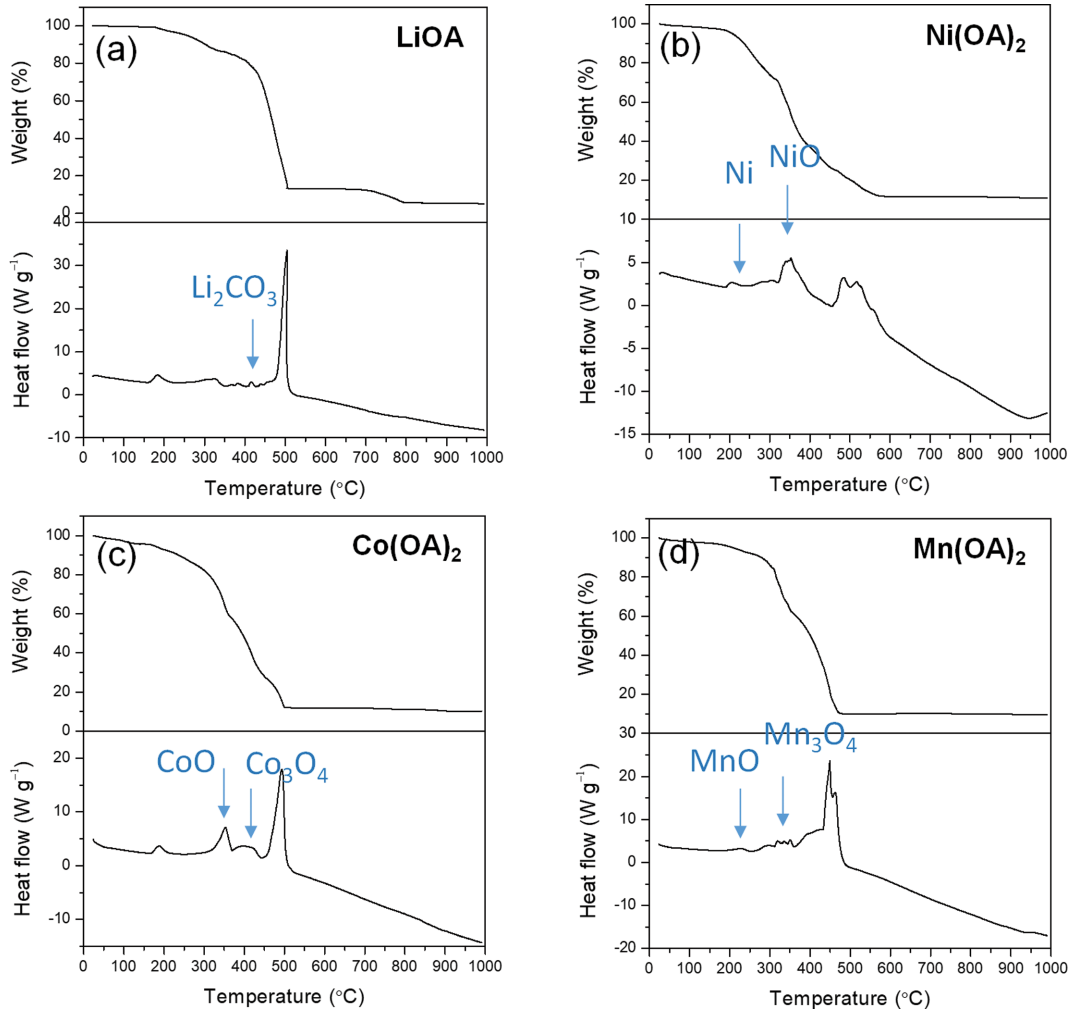

Fig. 3. TGA-DSC plots of (a) LiOA, (b) $Ni(OA)_2$, (c) $Co(OA)_2$, and (d) $Mn(OA)_2$ precursors measured at a heating rate of 10 °C min^{-1} in dry air.

Table 1. The Rietveld refinement results for the XRD patterns of NCM-Ac and NCM-OA calcined at 950 °C for 3 h under air

Sample	$I_{(003)}/I_{(104)}$	$(I_{(006)}+I_{(102)})/I_{(101)}$	Lattice parameters			Rietveld refinement results			
			a [Å]	*c* [Å]	*c*/*a*	R_p	R_{wp}	R_{exp}	χ^2
NCM-Ac	1.64	0.445	2.8538	14.2078	4.9786	9.56	10.2	5.25	3.75
NCM-OA	1.85	0.477	2.8586	14.2394	4.9812	13.3	13.7	5.42	6.41

ion mixing introduces a structural deformation into the NiO-like electrochemically inactive $Fm\bar{3}m$ phase; furthermore, Ni cations in Li^+ slabs hinder Li^+ diffusion during the charge/discharge process. In general, the intensity ratio between the (003) and (104) diffraction peaks is used to assess the degree of cation mixing, where a larger $I_{(003)}/I_{(104)}$ ratio indicates a lower degree of cation mixing [27, 49]. The $I_{(003)}/I_{(104)}$ ratio of NCM-OA was compared with that of NCM-Ac, which was prepared by calcining a mixture of metal acetate precursors. As shown in Table 1, the $I_{(003)}/I_{(104)}$ value of 1.85 obtained from the XRD pattern of NCM-OA is substantially greater than obtained from the pattern of NCM-Ac (1.64), which means that cation mixing of Ni in the Li^+ slab is suppressed when the solid-state conversion reaction is performed with a homogeneous mixture of metal oleate precursors. This suppression leads to better electrochemical performance in terms of capacity and cycling life (the electrochemical performance is discussed later). In addition, the splitting of peaks into the (006) and (102) and into the (018) and (110) diffractions becomes more pronounced with increasing distortion along the *c*-axis in the cubic close-packing structure by the sublattice of oxygen array [50-52]. For example, Qilu et al. used the $(I_{(006)}+I_{(102)})/I_{(101)}$ ratio as a figure of merit for estimating the $R\bar{3}m$ crystal structure [53]. As shown in Table 1, the $(I_{(006)}+I_{(102)})/I_{(101)}$ ratio of NCM-OA (0.477) is larger than that of NCM-Ac (0.445). The *c*/*a* ratios for NCM-OA and NCM-Ac by the Rietveld analysis were calculated to be 4.9812 and 4.9786, respectively, as provided in Table 1 and Fig. S2. The lattice parameter *c*, which is aligned with the *z*-axis, represents the average interplanar distance between metal slabs; thus, larger *c*/*a* ratio reflects the

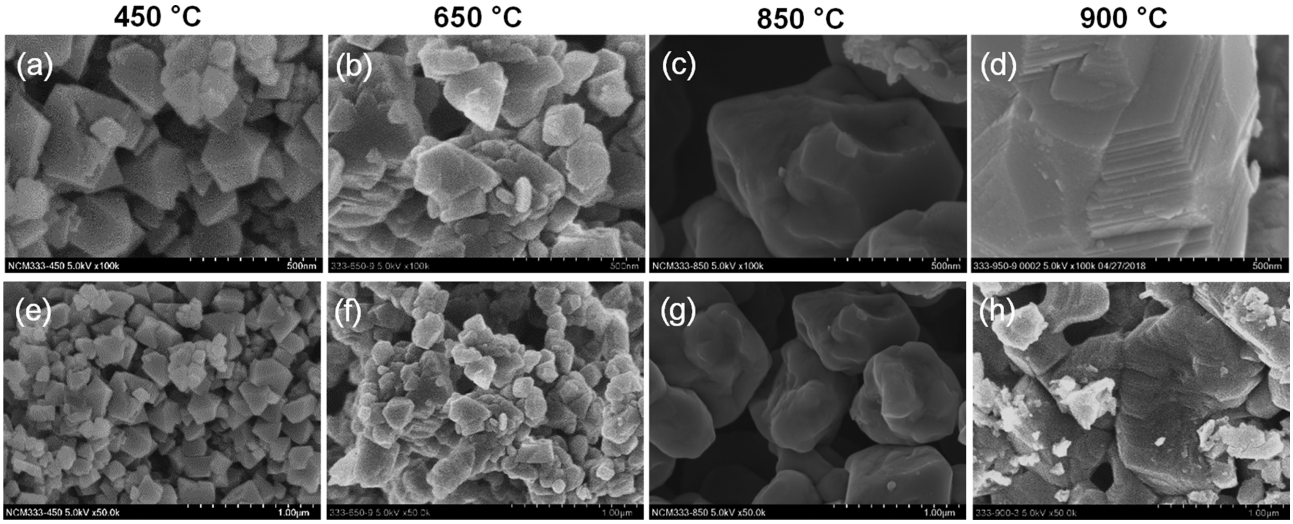

Fig. 4. SEM images of (a)-(d) NCM-OA and (e)-(h) NCM-Ac calcined at different temperatures.

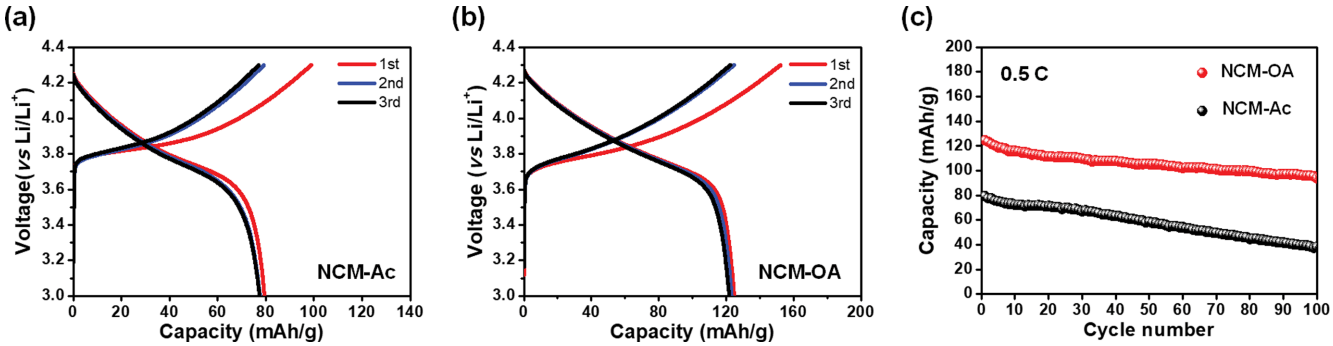

Fig. 5. Initial galvanostatic charge/discharge voltage profile of (a) NCM-Ac and (b) NCM-OA estimated at 0.5C. (c) Cycle performances of the corresponding samples shown in (a) and (b) obtained at 0.5C.

well-developed trigonal distortion of the hexagonal layered structure [27]. The Rietveld refinement results show that 0.127% of Ni is located in the 3b sites of the Li slab in NCM-Ac, whereas all of the Ni cations occupy the 3a in the transition-metal slab in NCM-OA. On the basis of all of the aforementioned crystal structure analysis results, we concluded that the use of a highly homogeneous metal oleate precursor mixture has the advantage of producing a well-defined $R\bar{3}m$ crystal structure of NCM333 because of the precursors' fluidic behavior at low temperatures.

Fig. 4 shows SEM images of NCM-OA and NCM-Ac samples calcined at different temperatures. Relatively well-defined morphologies are observed as the calcination temperature is increased from 450 °C to 900 °C. During formation of the layered structure, small particles merge to form larger particles. Contrary to the NCM-OA, NCM-Ac forms irregular-shaped particles with a broad size distribution. The regular and conformal shape of the active materials provides greater energy density per unit volume and therefore contributes to the development of a lightweight power source with high energy density. The average particle sizes of NCM-Ac and NCM-OA are 534 and 532 nm, respectively. Crystallite sizes along [003] direction calculated by Debye-Scherrer equation ($t=0.9\lambda/B\cos\theta$, where t is the mean crystallite size, λ is the X-ray wavelength, B is the full width at half maximum, and θ is the Bragg angle) are 46.6 and 56.4 nm for NCM-Ac and NCM-OA.

2. Electrochemical Properties $LiNi_{1/3}Co_{1/3}Mn_{1/3}O_2$

Fig. 5(a) and (b) shows the initial galvanostatic charge/discharge voltage profiles of NCM-Ac and NCM-OA samples at 0.5C. Fig. 5(c) shows the discharge capacity curves of NCM-Ac and NCM-OA at 0.5C (100 mA h g^{-1}) between 3.0 and 4.3 V. The initial discharge capacities of NCM-Ac and NCM-OA were 79.50 mA h g^{-1} and 124.80 mA h g^{-1}, respectively, at the first activation step. Their coulombic efficiencies were 80.41% and 82.07%, respectively. After the hundredth cycle, the discharge capacities of NCM-Ac and NCM-OA decreased to 38.24 mA h g^{-1} and 94 mA h g^{-1}, respectively. The capacity retention of the two samples, as calculated from the discharge capacity at the first and 100th cycles, was 48.10% and 75.38%, respectively. The NCM-OA exhibits a higher capacity and greater coulombic efficiency than the NCM-Ac at the initial cycles and better capacity retention after a hundred cycles.

Similar trends of the rate capabilities of NCM-Ac and NCM-OA at 0.2C-10C are evident in Fig. 6. NCM-OA exhibits discharge capacities ranging from 166.33 mA h g^{-1} (0.2C) to 74.46 mA h g^{-1} (2C), whereas NCM-Ac exhibits capacities ranging from 80.98 mA h g^{-1} (0.2C) to 38.84 mA h g^{-1} (2C). Thus, the discharge capac-

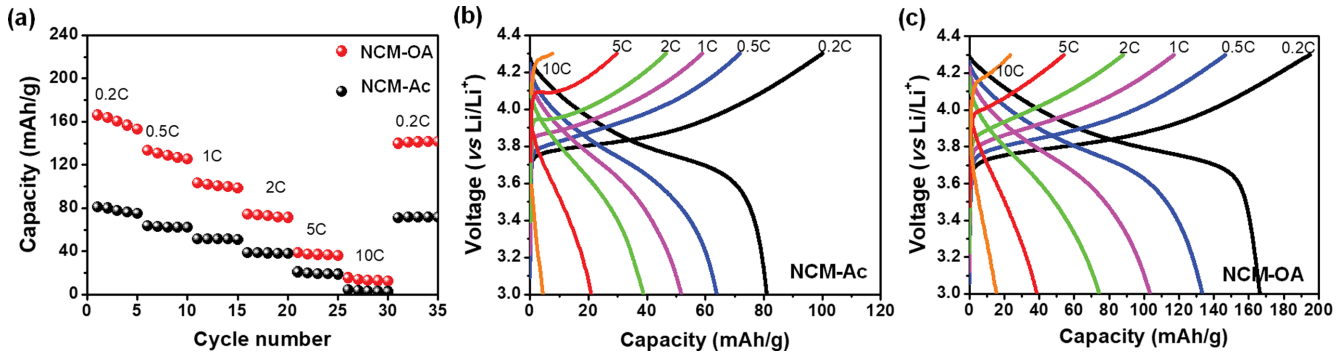

Fig. 6. (a) Rate capabilities of samples at current densities from 0.2C to 10C. Initial galvanostatic charge/discharge voltage profile of (a) NCM-Ac and (b) NCM-OA obtained at different C-rates (0.2C-10C).

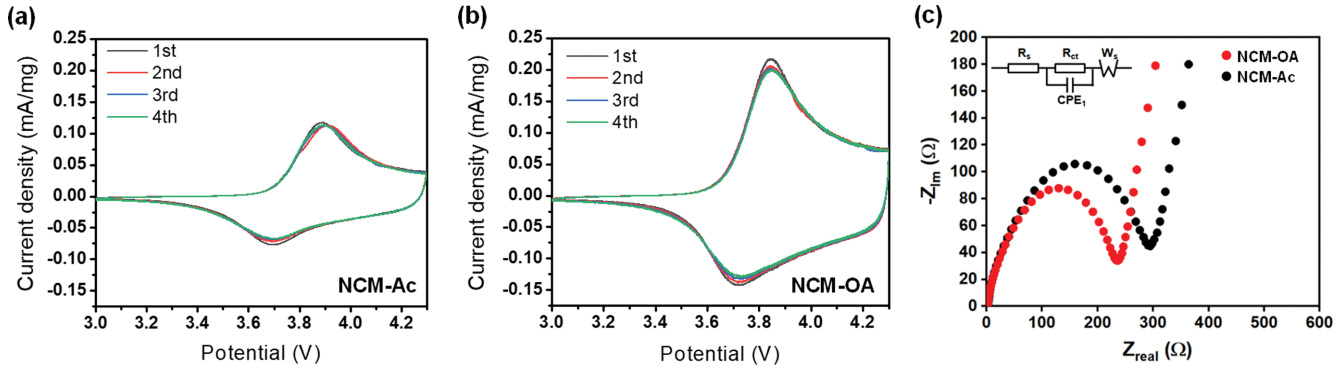

Fig. 7. CV curves of (a) NCM-Ac and (b) NCM-OA at a scan rate of 0.1 mV s^{-1}. (c) Nyquist plots of NCM-OA and NCM-Ac after 3 cycles. Inset image represents the equivalent circuit for fitting the impedance spectra.

ity of NCM-OA is almost twice that of NCM-Ac. The coulombic efficiencies of NCM-OA at the corresponding aforementioned C-rates ranged from 85.63 (0.2C) to 94.09% (2C), which are greater than those of NCM-Ac (81.03-83.56%). These superior electrochemical properties of NCM-OA compared with those of NCM-Ac are a consequence of the high crystallinity and suppressed cation mixing of its $R\bar{3}m$ layered structure.

To investigate the electrochemical reversibility and kinetic behavior, CV analysis was performed, as shown in Fig. 7(a) and (b). The CV tests of NCM-Ac and NCM-OA samples were conducted in the voltage range from 3.0 to 4.3 V at a scan rate of 0.1 mV s^{-1} for the first four cycles. Both CV curves exhibit a typical pair of redox peaks corresponding to the Ni^{2+}/Ni^{4+} redox couple between 3.7 and 3.9 V [54,55]. Although the CV curves of the two samples show similar redox peaks, the curve of the NCM-OA sample shows a sharper peak and larger anodic and cathodic peak currents (I_{ap}, I_{cp}) than that of the NCM-Ac sample. The anodic/cathodic peak current densities of NCM-OA (–0.142/0.216 mA mg^{-1}) are larger than that of NCM-Ac (–0.076/0.117 mA mg^{-1}). This difference indicates that the NCM-OA cathode exhibits good reversibility, small electrode polarization, and high electrochemical redox reaction activity. As cycling progresses, the peak current intensity slowly decreases, resulting in very slight capacity fade. The potential difference between the anodic/cathodic peaks represents the reversibility of the Li^+-ion intercalation and deintercalation process, where a larger value indicates greater electrode polarization [56,57]. The potential difference of NCM-OA is 0.13 V, which is smaller than that of NCM-Ac (0.21 V).

To further investigate the effect of using metal oleate precursors, electrochemical impedance spectroscopy (EIS) analysis was performed after three cycles (Fig. 7(c)). Nyquist plots of NCM-OA and NCM-Ac consist of small intercept in high frequency region assigned to electrolyte resistance (R_s), semicircle in high to medium frequency region assigned to charge transfer resistance (R_{ct}), and sloped line in low frequency region assigned to Warburg impedance (W_s). The R_{ct} value of NCM-OA (227.5 Ω) is lower than that of NCM-Ac (283.9 Ω), indicating that the Li^+/Ni^{2+} cation mixing is inhibited in NCM-OA, thereby reducing the barrier of Li^+ transfer [58].

The superior electrochemical performance of the NCM-OA to NCM-Ac may result from perfect arrangement of cations within the $R\bar{3}m$ layered structure. In the case of NCM-OA, all of the Ni cations being positioned at 3a sites facilitates the diffusion of Li^+ cations, whereas Ni cations in the Li slab blocks Li^+ cation diffusion in NCM-Ac. Moreover, Ni cations at 3b sites convert the layered structure into spinel and even less electro-active rock-salt structures, compromising the cyclic ability during prolonged charging and discharging. For this reason, NCM-OA exhibits longer cycle life than NCM-Ac by suppressing the formation of spinel or rock-salt crystals on the surface of the layered structure.

CONCLUSIONS

NCM333 was successfully synthesized as a cathode-active material for LIBs with metal-oleate precursors via a solid-state reaction. These metal oleate precursors have low melting temperatures, which facilitates homogeneous mixing at the molecular level. The process employing metal oleate precursors does not require a separate step to maximize the homogeneous distribution of solid-state precursors for calcination, such as a ball-milling process. The produced NCM-OA sample with NCM333 composition exhibited a well-defined $R\bar{3}m$ layered hexagonal structure. XRD analysis by Rietveld refinement shows that all of the Ni cations were located in the 3a sites of the transition-metal slab. This complete layered crystal formation led to enhanced electrochemical performance during cycling tests. We believe that the method of using metal-oleates represents an economical process for the production of high-quality cathode materials at industrial scale.

ACKNOWLEDGEMENTS

This study was supported by Korea Agency for Infrastructure Technology Advancement (Grant No. 19POQW-B152733-01).

SUPPORTING INFORMATION

Additional information as noted in the text. This information is available via the Internet at http://www.springer.com/chemistry/journal/11814.

REFERENCES

1. M. Armand and J.-M. Tarascon, *Nature*, **451**, 652 (2008).
2. J.-M. Tarascon and M. Armand, *Nature*, **414**, 359 (2001).
3. J. F. Peters, M. Baumann, B. Zimmermann, J. Braun and M. Weil, *Renew. Sustain. Energy Rev.*, **67**, 491 (2017).
4. L. Su, Y. Jing and Z. Zhou, *Nanoscale*, **3**, 3967 (2011).
5. F. Cheng, J. Liang, Z. Tao and J. Chen, *Adv. Mater.*, **23**, 1695 (2011).
6. W.-G. Lim, C. Jo, J. Lee and D. S. Hwang, *Korean J. Chem. Eng.*, **35**, 579 (2018).
7. J.-E. Lim and J.-K. Kim, *Korean J. Chem. Eng.*, **35**, 2464 (2018).
8. X. Cui, S. Wang, L. Mao, P. Wang, Z. Li, S. Wang and S. Li, *Electrochim. Acta*, **337**, 135709 (2020).
9. H. S. Ko, H. W. Park, G. J. Kim and J. D. Lee, *Korean J. Chem. Eng.*, **36**, 620 (2019).
10. F. Schipper, E. M. Erickson, C. Erk, J.-Y. Shin, F. F. Chesneau and D. Aurbach, *J. Electrochem. Soc.*, **164**, A6220 (2017).
11. D.-L. Vu and J.-w. Lee, *Korean J. Chem. Eng.*, **33**, 514 (2016).
12. Y. Wang, Y. Chen, S. Cheng and L. He, *Korean J. Chem. Eng.*, **28**(3), 964 (2011).
13. C.-H. Doh, B.-S. Jin, J.-H. Lim and S.-I. Moon, *Korean J. Chem. Eng.*, **19**, 749 (2002).
14. S. Li, K. Zhu, J. Liu, D. Zhao and X. Cui, *J. Electrochem. Energy*, **16**, 011006 (2019).
15. J. Wang, X. Yao, X. Zhou and Z. Liu, *J. Mater. Chem.*, **21**, 2544 (2011).
16. Y.-J. Shin, W.-J. Choi, Y.-S. Hong, S. Yoon, K. S. Ryu and S. H. Chang, *Solid State Ionics*, **177**, 515 (2006).
17. R. Santhanam and B. Rambabu, *J. Power Sources*, **195**, 4313 (2010).
18. M. G. Kim, H. J. Shin, J.-H. Kim, S.-H. Park and Y.-K. Sun, *J. Electrochem. Soc.*, **152**, A1320 (2005).
19. Y. Idemoto and T. Matsui, *Solid State Ionics*, **179**, 625 (2008).
20. F. Wu, M. Wang, Y. Su, L. Bao and S. Chen, *J. Power Sources*, **195**, 2900 (2010).
21. K.-S. Lee, S.-T. Myung and Y.-K. Sun, *J. Power Sources*, **195**, 6043 (2010).
22. J. Li, C. Cao, X. Xu, Y. Zhu and R. Yao, *J. Mater. Chem. A*, **1**, 11848 (2013).
23. Y. Fujii, H. Miura, N. Suzuki, T. Shoji and N. Nakayama, *J. Power Sources*, **171**, 894 (2007).
24. Z. Chang, Z. Chen, F. Wu, X.-Z. Yuan and H. Wang, *Electrochim. Acta*, **54**, 6529 (2009).
25. C. Yu, G. Li, X. Guan, J. Zheng, L. Li and T. Chen, *Electrochim. Acta*, **81**, 283 (2012).
26. N. Kiziltas-Yavuz, M. Herklotz, A. M. Hashem, H. M. Abuzeid, B. Schwarz, H. Ehrenberg, A. Mauger and C. M. Julien, *Electrochim. Acta*, **113**, 313 (2013).
27. Z.-D. Huang, X.-M. Liu, S.-W. Oh, B. Zhang, P.-C. Ma and J.-K. Kim, *J. Mater. Chem.*, **21**, 10777 (2011).
28. C. Li, Q. Hou, S. Li, F. Tang and P. Wang, *J. Alloys Compd.*, **723**, 887 (2017).
29. W.-H. Ryu, S.-J. Lim, W.-K. Kim and H.-S. Kwon, *J. Power Sources*, **257**, 186 (2014).
30. F. Wu, M. Wang, Y. Su, L. Bao and S. Chen, *J. Power Sources*, **195**, 2362 (2010).
31. J. Xie, X. Huang, Z. Zhu and J. Dai, *Ceram. Int.*, **36**, 2485 (2010).
32. N. N. Sinha and N. Munichandraiah, *J. Electrochem. Soc.*, **157**, A647 (2010).
33. K. M. Shaju and P. G. Bruce, *Adv. Mater.*, **18**, 2330 (2006).
34. C. X. Ding, Q. S. Meng, L. Wang and C. H. Chen, *Mater. Res. Bull.*, **44**, 492 (2009).
35. Y. Ding, P. Zhang, Z. Long, Y. Jiang and D. Gao, *J. Alloys Compd.*, **462**, 340 (2008).
36. C.-H. Lu and Y.-K. Lin, *J. Power Sources*, **189**, 40 (2009).
37. J.-W. Lee, J.-H. Lee, T. T. Viet, J.-Y. Lee, J.-S. Kim and C.-H. Lee, *Electrochim. Acta*, **55**, 3015 (2010).
38. X. Jiang, Y. Sha, R. Cai and Z. Shao, *J. Mater. Chem. A*, **3**, 10536 (2015).
39. P. He, H. Wang, L. Qi and T. Osaka, *J. Power Sources*, **160**, 627 (2006).
40. D.-C. Li, T. Muta, L.-Q. Zhang, M. Yoshio and H. Noguchi, *J. Power Sources*, **132**, 150 (2004).
41. L. Q. Wang, L. F. Jiao, H. Yuan, J. Guo, M. Zhao, H. X. Li and Y. M. Wang, *J. Power Sources*, **162**, 1367 (2006).
42. T. Ohzuku and Y. Makimura, *Chem. Lett.*, **30**, 642 (2001).
43. Y. Huang, J. Chen, J. Ni, H. Zhou and X. Zhang, *J. Power Sources*, **188**, 538 (2009).
44. N. Yabuuchi and T. Ohzuku, *J. Power Sources*, **119-121**, 171 (2003).
45. I. Belharouak, Y.-K. Sun, J. Liu and K. Amine, *J. Power Sources*, **123**, 247 (2003).
46. J. Park, K. An, Y. Hwang, J.-G. Park, H.-J. Noh, J.-Y. Kim, J.-H. Park, N.-M. Hwang and T. Hyeon, *Nat. Mater.*, **3**, 891 (2004).
47. J. Rodriguez-Carvajal, *Physica B*, **192**, 55 (1993).
48. T. Roisnel and J. Rodriguez-Carvajal, *Mater. Sci. Forum*, **378-381**, 118 (2001).

49. J. Breger, N. Dupre, P. J. Chupas, P. L. Lee, T. Proffen, J. B. Parise and C. P. Grey, *J. Am. Chem. Soc.*, **127**, 7529 (2005).
50. T. Ohzuku, K. Nakura and T. Aoki, *Electrochim. Acta*, **45**, 151 (1999).
51. B. Zhang, G. Chen, P. Xu and C. C. Li, *J. Power Sources*, **176**, 325 (2008).
52. C. Deng, S. Zhang, B. Wu, S. Y. Yang and H. Q. Li, *J. Solid State Electrochem.*, **14**, 871 (2010).
53. X. Zhang, W. J. Jiang, A. Mauger, Qilu, F. Gendron and C. M. Julien, *J. Power Sources*, **195**, 1292 (2010).
54. E. Zhao, M. Chen, D. Chen, X. Xiao and Z. Hu, *ACS Appl. Mater. Interfaces*, **7**, 27096 (2015).
55. C. Yang, X. Zhang, M. Huang, J. Huang and Z. Fang, *ACS Appl. Mater. Interfaces*, **9**, 12408 (2017).
56. J.-H. Park, J.-H. Cho, S.-B. Kim, W.-S. Kim, S.-Y. Lee and S.-Y. Lee, *J. Mater. Chem.*, **22**, 12574 (2012).
57. L.-L. Zhang, Z. Li, X.-L. Yang, X.-K. Ding, Y.-X. Zhou, H.-B. Sun, H.-C. Tao, L.-Y. Xiong and Y.-H. Huang, *Nano Energy*, **34**, 111 (2017).
58. Q. Zhang, Y. Su, L. Chen, Y. Lu, L. Bao, T. He, J. Wang, R. Chen, J. Tan and F. Wu, *J. Power Sources*, **396**, 734 (2018).

Supporting Information

Solid-state conversion of metal oleate precursors for the preparation of $LiNi_{1/3}Co_{1/3}Mn_{1/3}O_2$ as cathode material for lithium-ion batteries

Dongyub Kwak*,‡, Won-Gwang Lim,‡, Kyuchul Shin*, In Woo Cheong*,†, Jinwoo Lee**,†, and Jin Joo*,†**

*Department of Applied Chemistry, Kyungpook National University, Daegu 41566, Korea
**Department of Chemical and Biomolecular Engineering, Korea Advanced Institute of Science and Technology (KAIST), Daejeon 34141, Korea

(*Received 19 January 2020 • Revised 5 March 2020 • Accepted 8 March 2020*)

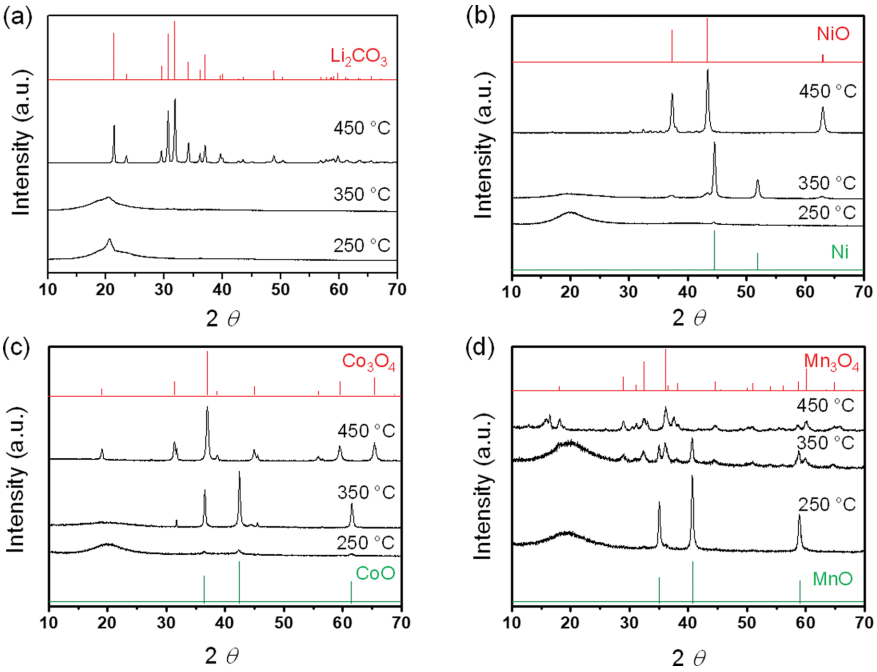

Fig. S1. XRD patterns of metal oleate precursors (a) LiOA, (b) $Ni(OA)_2$, (c) $Co(OA)_2$, and (d) $Mn(OA)_2$ calcined at 250 °C, 350 °C and 450 °C.

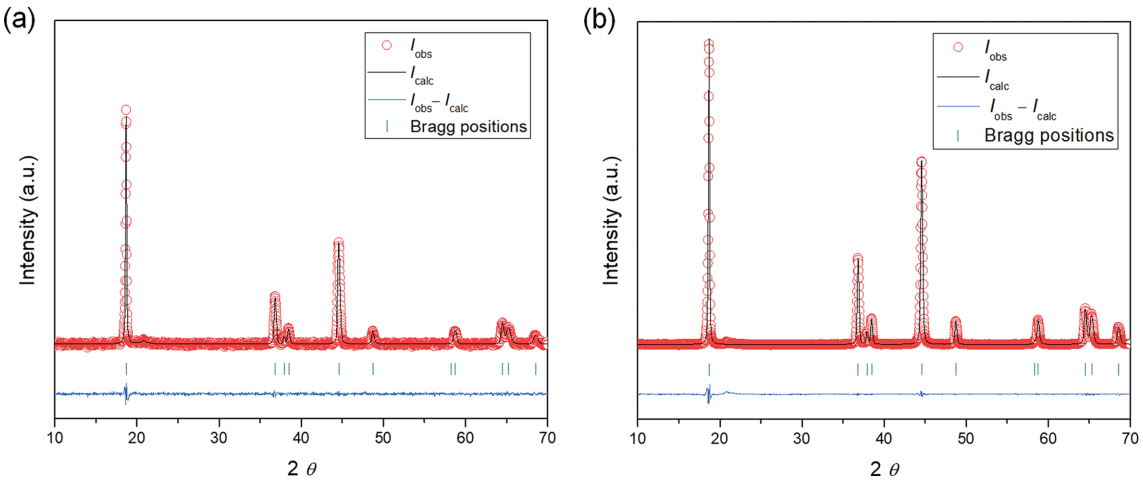

Fig. S2. The Rietveld refinement for the XRD patterns of (a) NCM-OA and (b) NCM-Ac.